



Interleukin-17-mediated protective cytokine signaling against degeneration of the retinal pigment epithelium

Yan Chen^a , Sarah E. Bounds^b , Xiang Ma^c, James Regun Karmoker^b , Yin Liu^d, Jian-Xing Ma^c, and Jiyang Cai^{b,1}

Edited by Andrew J. Lotery, University of Southampton, Southampton; received July 9, 2023; accepted November 7, 2023 by Editorial Board Member Jeremy Nathans

Injuries to the retinal pigment epithelium (RPE) and outer retina often result in the accumulation of retinal microglia within the subretinal space. These subretinal microglia play crucial roles in inflammation and resolution, but the mechanisms governing their functions are still largely unknown. Our previous research highlighted the protective functions of choroidal $\gamma\delta$ T cells in response to RPE injury. In the current study, we employed single-cell RNA sequencing approach to characterize the profiles of immune cells in mouse choroid. We found that $\gamma\delta$ T cells were the primary producer of interleukin-17 (IL-17) in the choroid. IL-17 signaled through its receptor on the RPE, subsequently triggering the production of interleukin-6. This cascade of cytokines initiated a metabolic reprogramming of subretinal microglia, enhancing their capacity for lipid metabolism. RPE-specific knockout of IL-17 receptor A led to the dysfunction of subretinal microglia and RPE pathology. Collectively, our findings suggest that responding to RPE injury, the choroidal $\gamma\delta$ T cells can initiate a protective signaling cascade that ensures the proper functioning of subretinal microglia.

age-related macular degeneration | microglia | cytokine

The immune privilege of ocular tissues shields the neural retina from inflammation and immune responses (1). Few lymphocytes are present in the retina when the blood–retinal barrier is intact, even under early disease conditions such as degeneration of the retina and/or retinal pigment epithelium (RPE) (2). The possible mechanisms supporting immune privilege include 1) no defined classical lymphatic system that drains the posterior segment of the eye, although a glymphatic system has been recently identified in rodent eye (3); 2) multiple suppressive cytokines, such as transforming growth factor b (TGF-b), that inhibit effector T cells and promote Treg function (4); and 3) Fas ligand expressed in RPE cells that may trigger apoptotic T cell death when T cells reach the epithelial barrier (5).

The immunosuppressive milieu also inhibits the function of myeloid cells such as the retinal microglia. Under physiological conditions, microglia are localized in the inner and outer plexiform layers (6). In response to injuries to the RPE and photoreceptor cells, microglia migrate to the pathogenic niche of subretinal space and facilitate the RPE to remove debris and metabolic waste products. Depletion of microglia can worsen RPE and photoreceptor injury (6, 7). The microenvironment along the migration path of microglia is highly suppressive and the subretinal microglia need to be rejuvenated in order to perform their functions effectively. How the local immune modulatory mechanisms work to support microglial function in this pathological niche remains largely unclear (8).

Unlike the retina, the choroid does not have immune privilege. We previously reported that choroidal $\gamma\delta$ T cells can be activated responding to both acute and chronic stress to the RPE, and exert protective functions (9, 10). Mice with $\gamma\delta$ T cell deficiency are more vulnerable to sodium iodate (NaIO_3), which selectively damages the RPE (11, 12). In line with this, adoptive transfer of wild-type $\gamma\delta$ T cells to animals lacking the T cell receptor (TCR) delta chain increased their resistance to NaIO_3 (9), further supporting the protective roles of choroidal $\gamma\delta$ T cells in maintaining the outer retina homeostasis.

The goal of the current study is to investigate the mechanisms underlying the protective functions of choroidal $\gamma\delta$ T cells. Our findings revealed that IL-17 (interleukin-17), which is primarily produced by $\gamma\delta$ T cells in the mouse choroid, can trigger the RPE to produce IL-6 (interleukin-6). IL-6 can metabolically reprogram the microglia by activating the mechanistic target of rapamycin (mTOR). RPE-specific deletion of the IL-17 receptor A (IL17RA) caused dysfunction of both the RPE and subretinal microglia. The data collectively indicate that the RPE can relay the cytokine signals from $\gamma\delta$ T cells in the choroid to microglia in the subretinal space. This protective cytokine network revives the microglial function at the site with RPE injury.

Significance

Retinal microglia in the subretinal niche have protective functions against injuries to the retinal pigment epithelium (RPE), yet their overactivation can cause neuronal damage. The current research focused on unraveling a signaling network involving choroidal $\gamma\delta$ T cells-produced IL-17 (interleukin-17) and RPE-produced IL-6 (interleukin-6). This network was found to be instrumental in metabolically reprogramming subretinal microglia, offering insights into the mechanisms governing their controlled activation.

Author affiliations: ^aDepartment of Ophthalmology, Dean McGee Eye Institute, University of Oklahoma Health Sciences Center, Oklahoma City, OK 73104; ^bDepartment of Physiology, University of Oklahoma Health Sciences Center, Oklahoma City, OK 73104; ^cDepartment of Biochemistry, Wake Forest University School of Medicine, Winston-Salem, NC 27157; and ^dDepartment of Neurobiology and Anatomy, University of Texas Health Science Center at Houston, Houston, TX 77030

Author contributions: Y.C. and J.C. designed research; Y.C., S.E.B., X.M., J.R.K., and J.C. performed research; X.M., Y.L., and J.C. contributed new reagents/analytic tools; Y.C., X.M., Y.L., J.-X.M., and J.C. analyzed data; and Y.C., J.-X.M., and J.C. wrote the paper.

The authors declare no competing interest.

This article is a PNAS Direct Submission. A.J.L. is a guest editor invited by the Editorial Board.

Copyright © 2023 the Author(s). Published by PNAS. This article is distributed under [Creative Commons Attribution-NonCommercial-NoDerivatives License 4.0 \(CC BY-NC-ND\)](#).

¹To whom correspondence may be addressed. Email: jiyang-cai@ouhsc.edu.

This article contains supporting information online at <https://www.pnas.org/lookup/suppl/doi:10.1073/pnas.2311647120/-DCSupplemental>.

Published December 12, 2023.

Results

RPE Injury Activated an Immune Regulatory Axis of IL-17-RPE-IL-6. In our previous study, we observed an increase in the number of choroidal $\gamma\delta$ T cells in response to RPE injury induced by NaIO₃ (9). With flow cytometry analyses and using gates defined by splenic $\gamma\delta$ T cells (Fig. 1 A–C), we found that over 35% ($36.95 \pm 22.3\%$, mean \pm SD, N = 7) of the $\gamma\delta$ T cells in the choroid were capable of producing IL-17 (Fig. 1 D–I). To gain further insight into the characteristics of choroidal immune cells after NaIO₃ treatment, we enriched CD45-positive cells from RPE/choroid tissue using flow cytometry sorting and performed single-cell RNA sequencing (scRNA-seq) analysis. Unsupervised clustering analysis showed that CD45⁺ enrichment effectively removed RPE cells, stromal cells, neuronal cells, and endothelial cells while retaining myeloid and lymphoid cells (Fig. 1 J). Consistent with previous literature

reports (13) and our own findings (14), the choroidal immune cell population comprised T cells, B cells, NK cells, and myeloid cells, including microglia/macrophage/monocytes (Fig. 1 J and K).

$\gamma\delta$ T cells, characterized by the expression of the TCR γ chain and the transcription factor RAR-related orphan receptor gamma (encoded by the *Rorc* gene), formed a distinct cluster separate from other CD3⁺ T cells (Fig. 1 J and K). The transcription of the *Il17a* gene was primarily restricted to the $\gamma\delta$ T cell cluster (Fig. 1 K and L). In addition to activating the immune cells, NaIO₃ treatment is known to trigger classical and alternative pathways of complement activation (12, 15). We found a time-dependent increase of C3d deposition in the photoreceptor layer (*SI Appendix*, Fig. S1A) and upregulation of CD46 in the RPE (*SI Appendix*, Fig. S1B). Both proteins have immune modulatory functions that can bridge the innate and adaptive immune systems (16–18).

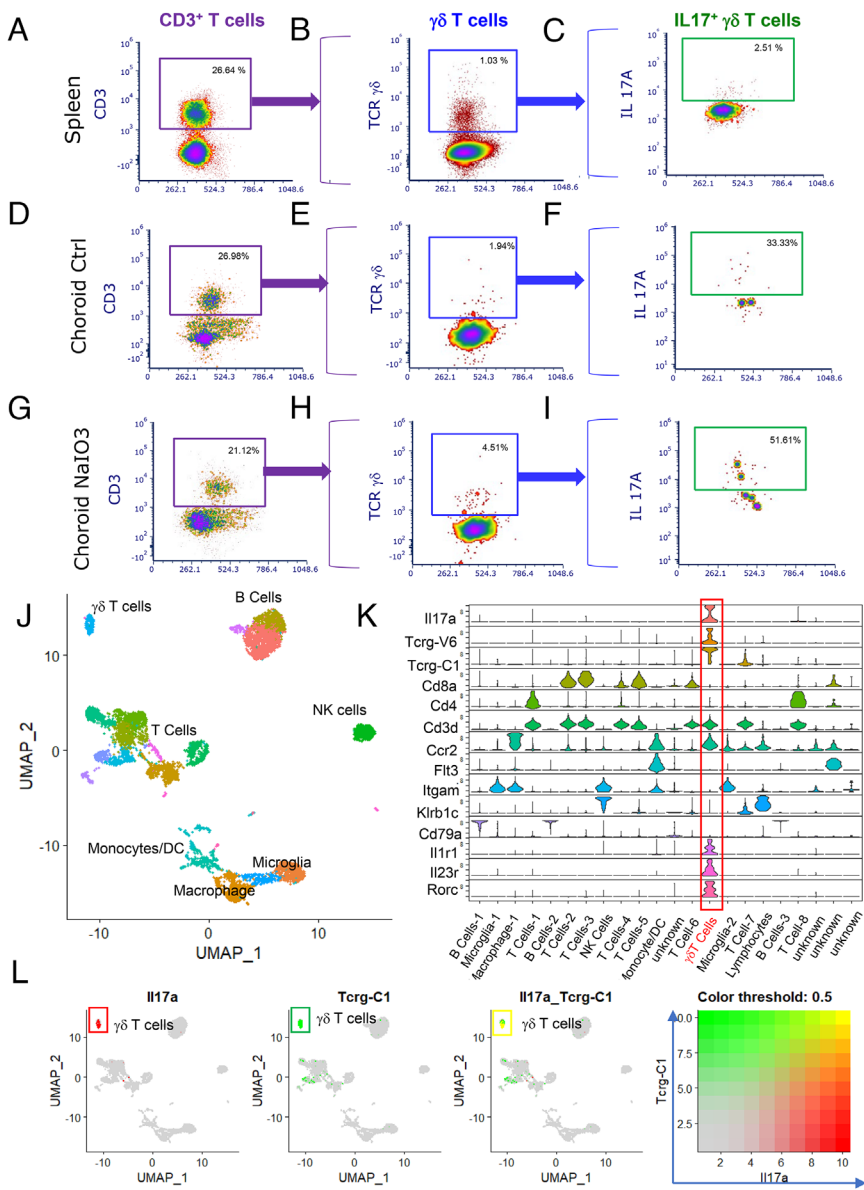


Fig. 1. IL-17-producing $\gamma\delta$ T cells in the choroid. (A–I) Flow cytometry analysis of IL-17⁺ $\gamma\delta$ T cells in the spleen and choroid of mice at 3 d after receiving NaIO₃ treatment at a dosage of 25 mg/kg body weight. The gates of CD3⁺ T cells, $\gamma\delta$ T cells, and IL-17-producing $\gamma\delta$ T cells were created using splenocytes (A–C) and applied to cells in the RPE/choroid preparations from control (D–F) and NaIO₃-treated mice (G–I). (J–L) scRNA-Seq analysis on RPE/choroid tissues enriched for CD45⁺ cells. The tissues were collected from pooled 4 eyes from NaIO₃-treated mice at 3 d after injection. (J) UMAP plot of single-cell clusters of CD45⁺ cells in RPE/choroid. (K) Violin plots of the expression level of marker genes in the single-cell clusters. The cluster expressing canonical markers of $\gamma\delta$ T cells is highlighted in the red box. (L) Feature plots of expression levels of *Il17a* and *Tcrg-C1* in single-cell clusters, with yellow indicating the coexpression of *Il17a* and *Tcrg-C1* in the cluster of $\gamma\delta$ T cells.

We performed immunofluorescence (IF) staining of IL-17A and $\gamma\delta$ T cells on paraffin sections of human posterior eyes, after antigen retrieval (Fig. 2A and *SI Appendix*, Fig. S2). Consistent with the previous observations (9), $\gamma\delta$ T cells were detected in various layers of the human choroid, including the choriocapillaris. Notably, a significant proportion of these cells showed positive staining of IL-17A, indicating that they are IL17-producing $\gamma\delta$ T cells. While the total number of $\gamma\delta$ T cells did not show a correlation with the patient disease status of age-related macular degeneration (AMD), we observed a decrease in the number of choroidal IL-17⁺ $\gamma\delta$ cells in the choroid of AMD eyes compared to age-matched control eyes (Fig. 2B).

IL-17A/F function through their receptor, which is a heterotrimeric complex of IL-17RA and IL-17RC (19). IL-17 RC is expressed by various cells in the outer retina, RPE, and choroid (20). When IL-17RA was examined by IF staining of the posterior mouse eye sections, it was found to be expressed mainly on the basal side of the RPE, similar to the distribution pattern of glucose transporter 1 (Fig. 2C) (21).

The expression of IL-17 receptor proteins by the RPE suggests that they may respond to the cytokine signals initiated by the choroidal $\gamma\delta$ T cells. With ex vivo organ culture of posterior eye cups with the RPE, we found that IL-17A was a potent stimulant of IL-6 production from the RPE (Fig. 2 D and E). Both the

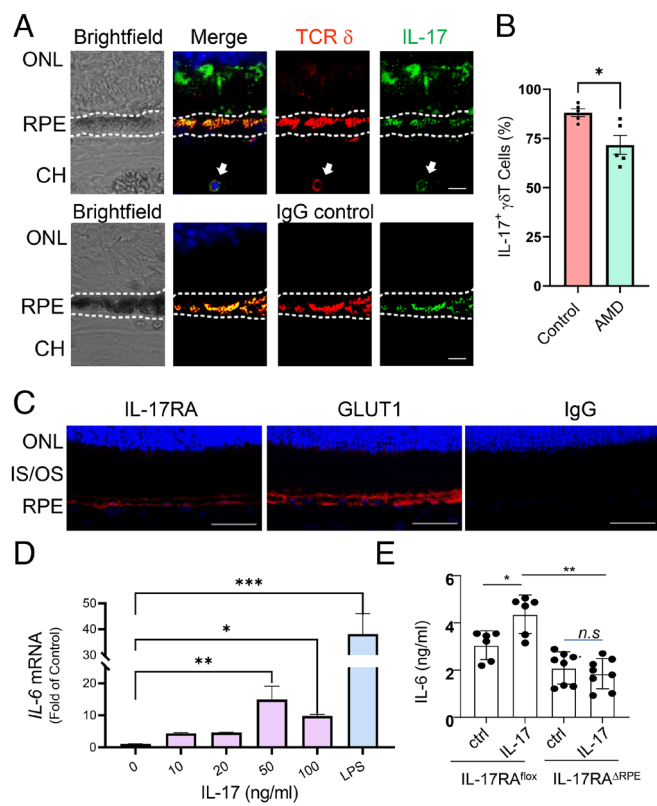


Fig. 2. IL-17-stimulated RPE IL-6 production (A) Immunostaining of paraffin sections of human posterior eye, from a control donor (73-Y-old, see F). The dashed line shows the position of the RPE. Green: IL-17; red: $\gamma\delta$ T. (B) Quantitation of IL17⁺ $\gamma\delta$ T cells in age-matched control and AMD subjects. (C) Representative images of IL-17 RA and GLUT1 immunostaining (Red) on cryosections of mice eye. Blue: nuclei (DAPI). The data presented are representatives of 5 independent experiments, using IL-17RA antibodies from different vendors. (D and E) IL17-stimulated IL-6 production from the RPE. The RPE/eye cups were incubated with IL-17A at the indicated concentrations for 6 h (mean \pm SD, N = 4). At the end of treatment, mRNA was prepared, and the level of *Il6* mRNA was determined by real-time qPCR (D). The IL-6 protein level in the conditioned media was determined with ELISA (E). [Scale bars: 10 mm (A) and 50 μ m (C)]. *P < 0.05; **P < 0.01; and ***P < 0.001.

mRNA level of the *Il6* gene and the IL-6 protein in the RPE-conditioned medium were up-regulated by IL-17. Similar results were obtained from cultured primary mouse RPE cells and ARPE-19 cells (*SI Appendix*, Fig. S3 A–D). The induction was specific for *Il6*, as other proinflammatory cytokine genes, such as *Il1b* and *Ccl2*, were not induced by IL-17 (*SI Appendix*, Fig. S3E). Similar RPE responses to IL-17 have been reported previously in autoimmune uveitis models (22).

IL-6 Metabolically Reprogrammed Microglia and Potentiated M2a Differentiation. IL-6 can have either protective or damaging effects in models of retinal injury (23, 24). We examined the effects of IL-6 on cultured primary retinal microglia (25). IL-6 was found to dose- and time-dependently activate the mTOR pathway and increase the phosphorylation of ribosome S6 protein, a surrogate of mTOR complex 1 activity (Fig. 3 A–D). As mTOR is a central regulator of cell metabolism, we used Seahorse metabolic flux assay to measure glucose- or fatty acid-dependent mitochondrial oxidative phosphorylation in cultured microglia. Primary microglia cells had active mitochondrial respiration (Fig. 3 E and F). IL-6 potently inhibited glucose- and glutamine-dependent mitochondrial oxidative phosphorylation (Fig. 3 E and F). The inhibition was dependent on mTOR complex 1, as pretreatment with rapamycin reversed the inhibitory effects of IL-6 on oxygen consumption. IL-6 also promoted fatty acid β -oxidation which is sensitive to inhibition of carnitine palmitoyltransferase 1 by etomoxir (Fig. 3 G and H), indicating a shift of mitochondrial fuel usage by retinal microglia toward long-chain fatty acid.

Next, we compared the transcriptome of the microglia with or without IL-6 exposure using bulk RNA sequencing. The differential gene expression analyses revealed a significant upregulation of the gene encoding IL-4 receptor alpha (*Il4ra*), also known as *Cd124*, upon IL-6 treatment (Fig. 4A). The upregulation of *Il4ra* was confirmed using real-time RT-PCR analyses. In cultured microglia, we observed a dose-dependent upregulation of *Il4ra* mRNA in response to IL-6 (Fig. 4B). Other subunits of the IL-4 receptor complex, such as IL-2RG or IL-13Ra1 (26, 27), were not induced by IL-6 (Fig. 4 C and D). The upregulation of CD124 by IL-6 was further verified using flow cytometry (Fig. 4 E and F). We also measured the changes in downstream signaling of IL-4 receptor. In cultured microglia, IL-4 treatment activated STAT6 phosphorylation, and such effect was potentiated by cotreatment with IL-6 (Fig. 4 G and H). IL-6 itself did not activate STAT6.

To determine the effects of these cytokines at the cellular functional level, we used flow cytometry analyses to assess the expression of CD206, a marker of polarized activation of myeloid cells (28). IL-4 and IL-6 both up-regulated CD206, and their combined effects were additive (Fig. 4I). These findings demonstrate that the RPE-produced IL-6 can reprogram microglia signaling pathways and cellular functions, thereby ensuring their activation status in the subretinal space.

RPE-Specific Knockout of IL-17RA Caused Subretinal Microglia Dysfunction. We used Bestrophin promoter-driven Cre (29) and IL-17RA floxed mice to generate RPE-specific knockout of the *Il17ra* gene. On fundus photos, the IL-17RA^{ΔRPE} mice showed RPE pigmentary changes and signs of retinal cell infiltration, which were aggravated with age (Fig. 5A). Rd8 mutation was not detected in these mice. When measured for the ERG (Electroretinography) c-wave response, the knockout mice had about 50% reduction in amplitude as compared to IL-17RA floxed mice and Best-Cre mice at 8 to 11 mo of age (Fig. 5B). The scotopic a-wave amplitudes showed a moderate decrease at high flash intensities, while the b-wave amplitudes were not affected

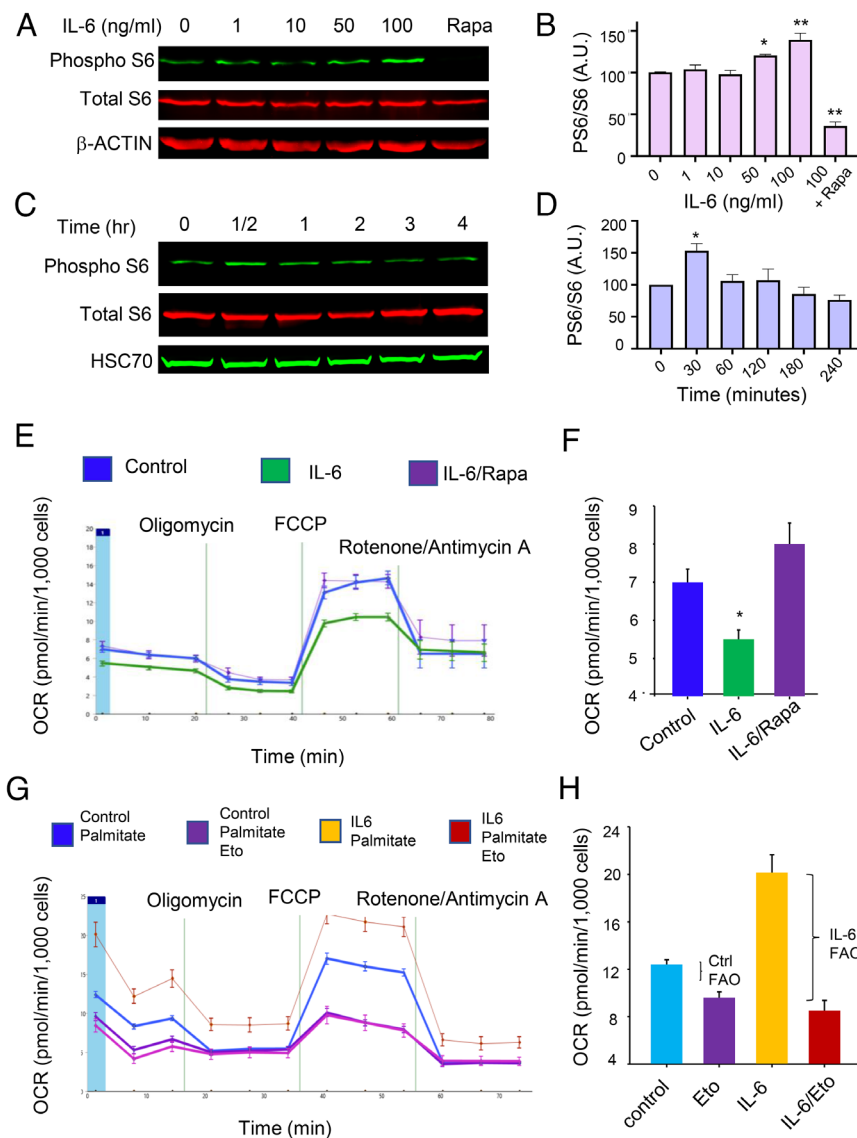


Fig. 3. Activation of microglia mTOR by IL-6. (A–D) Dose- and time-dependence of S6 phosphorylation in cultured primary retinal microglia treated with IL-6. Rapamycin (Rapa) at 20 nM was used as a control. (E and F) Seahorse Mito Stress Test in microglia treated with 50 ng/ml IL-6 or 20 nM rapamycin for 16 h. (G and H) Palmitate Oxidative Stress Test, using palmitate-BSA as substrate and etomoxir (Eto) as an inhibitor of mitochondrial long-chain fatty acid transporter. Oxygen consumption rates were calculated after normalization with the number of microglia cells in each well. Data presented are the average of 3 independent experiments (mean \pm SEM) (* $P < 0.05$ and ** $P < 0.01$).

by the IL-17RA knockout in the RPE (Fig. 5 C and D). OCT scan revealed no apparent retinal thinning (*SI Appendix*, Fig. S4). On paraffin sections (Fig. 5D), eyes from RPE-specific IL-17 RA knockout mice presented areas with subretinal cell infiltration, pigment loss, and focal thinning. On RPE/choroid flat mounts, IF staining showed that overexpression of Cre led to nearly 20% of the RPE cells with abnormal morphology (30), such as cells with more than two nuclei, no nucleus, or areas more than 3 times larger or smaller than the average size of cells in the midperipheral area. Knockout IL-17RA significantly increased the percentage of RPE cells with abnormal morphology (Fig. 3E). Thus, the loss of IL-17 signaling in the RPE negatively impacted the health of the RPE and outer retina.

Knockout IL-17RA abolished the IL-17-stimulated IL-6 production from the RPE (Fig. 2E). ScRNA seq analyses were performed to compare the gene expression profiles of CD45⁺ cells in RPE/choroid preparations from IL-17RA^{flx} and IL-17RA^{ΔRPE} mice. There were two clusters of immune cells with characteristic microglial markers of *Cd45* (*Ptprc*)⁺, *Cd11b* (*Itgam*)⁺, *Ccr2*^{low}, and

Cx3cr1⁺ (Fig. 6 A and B). Both of them represented subretinal microglia that were captured when the RPE/choroid tissues were collected. Gene ontology and pathway enrichment analyses identified multiple pathways that were differentially expressed between the subretinal microglial clusters from IL-17RA^{flx} and IL-17RA^{ΔRPE} mice (Fig. 6 C and D), and were related to immune modulation functions such as regulation of immune effector process and myeloid cell differentiation. Among them, we identified a number of candidate genes, such as *Apoe*, *Abcg1*, *Abca7*, and *Cd36*, that were involved in the lipid metabolism and were down-regulated in subretinal microglia of IL-17RA^{ΔRPE} mice (Fig. 6E). To validate the scRNA-seq data, we used magnetic-activated cell sorting (MACS) and CD11b antibody-conjugated beads to isolate mononuclear phagocytes from both retina and RPE/choroid fractions, followed by real-time RT-PCR analyses of gene expression. The results (Fig. 6F) showed that CD11b⁺ cells from the RPE/choroid of IL-17RA^{ΔRPE} mice had lower expression of lipid metabolism-related genes. We further used HSC LipidTox dye to stain for neutral lipid contents in CD45⁺ CD11b⁺ cells. In eyes from IL-17RA^{flx} mice,

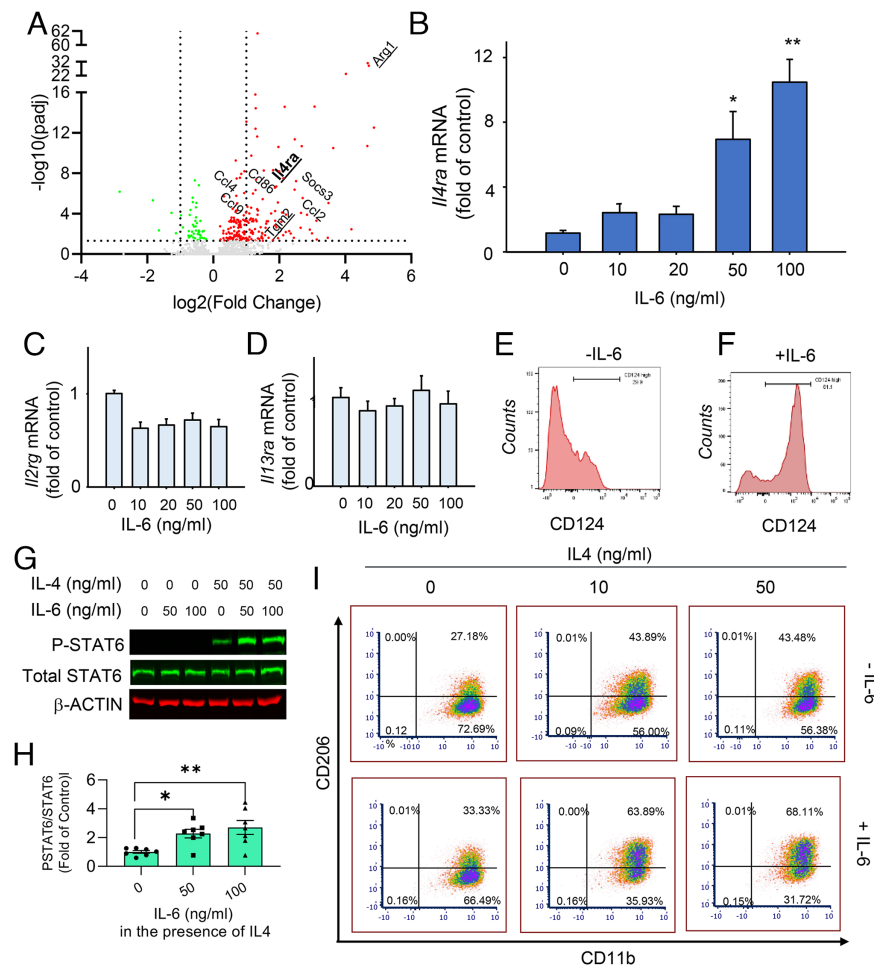


Fig. 4. IL-6 up-regulated microglial IL-4 signaling pathway. (A) Volcano plot showing differential gene expression as measured by bulk RNA-seq of cultured microglia with and without exposure to IL-6 at 50 ng/mL for 16 h. The *Il4ra* gene was highlighted. (B–D) Dose-dependent changes of mRNA levels of *Il4ra*, *Il2rg*, and *Il13ra* in response to IL-6 treatment in microglia (mean \pm SEM, $N = 3$). (E and F) Flow cytometry measurement and histogram plots of IL-4 RA (CD124) after IL-6 treatment. (G and H) Western blots of STAT 6 phosphorylation after treatment with IL-4 and IL-6. Data are representative of 3 independent experiments (mean \pm SEM) (* $P < 0.05$, ** $P < 0.01$). (I) Intracellular flow cytometry analyses of CD206 expression in microglia treated with IL-4 and IL-6 (representative of 3 independent experiments).

$28 \pm 6.0\%$ (mean \pm SD, $N = 3$) of CD11b $^+$ cells in the RPE/choroid fraction were positively stained for LipidTOX (31). The number went down to $17.2 \pm 5.4\%$ (mean \pm SD, $N = 3$) in cells isolated from IL-17RA ARPE mice. Thus, the subretinal microglia in mice with IL-17RA knockout in the RPE were less active in their functions related to lipid metabolism and were less efficient in the removal of waste products in the subretinal niche.

Discussion

$\gamma\delta$ T cells account for a small percentage of the total T cell pool (32), but become highly enriched at anatomical places with an epithelial barrier where they play critical roles in guarding the tissue integrity against infection and injury (33, 34). In the posterior eye, the RPE separates the choroidal blood supply from the retinal neurons. The presence of $\gamma\delta$ T cells in the choroid and choriocapillaris suggests that these cells can perform immune surveillance functions adjacent to the outer blood-retinal barrier. Similarly, meningeal IL-17 $^+$ $\gamma\delta$ T cells are associated with the blood-brain barrier and have been found to be important for cognitive functions (35, 36). Interactions among $\gamma\delta$ T cells, other immune cells, and epithelial tissue are integral components of inflammation and resolution in the central nervous system. Findings from our current study suggest that $\gamma\delta$ T cells control the cytokine milieu of the

microglia in the pathological niche of subretinal space and influence the functions of subretinal microglia.

In models of autoimmune uveitis, IL-17 $^+$ $\gamma\delta$ T cells regulate the antigen-presenting cells and the activation status of effector T cells (37, 38). Under conditions of sterile inflammation, in which no antigen-specific response is established, we found that acute and chronic RPE injury activated choroidal $\gamma\delta$ T cells and their IL-17 production (Fig. 1). While the underlying mechanisms remain to be determined, RPE can produce cytokines, such as IL-1 β (39), and endogenous ligands for aryl hydrocarbon (40) which can serve as activation signals to induce IL-17 production from $\gamma\delta$ T cells (41, 42). Injuries to the RPE also trigger complement activation (12, 15). Immune modulatory molecules, such as the cleavage products of complement proteins and CD46, can contribute to choroidal lymphocyte activation (16) by interacting with myeloid cells such as choroidal macrophages (43).

We found that in the posterior eye, IL-17 can serve as a protective cytokine (Fig. 5). The findings align with its known role in maintaining the intestinal epithelial integrity (44, 45). The number of IL-17 $^+$ $\gamma\delta$ T cells decreased in human AMD eyes (Fig. 2B). In AMD eyes, the functional interactions among RPE and choroidal immune cells can be lost with aging and disease, leading to an insufficient support from the $\gamma\delta$ T cells. Knockout of IL-17RA caused RPE pathology, as detected by fundus photo,

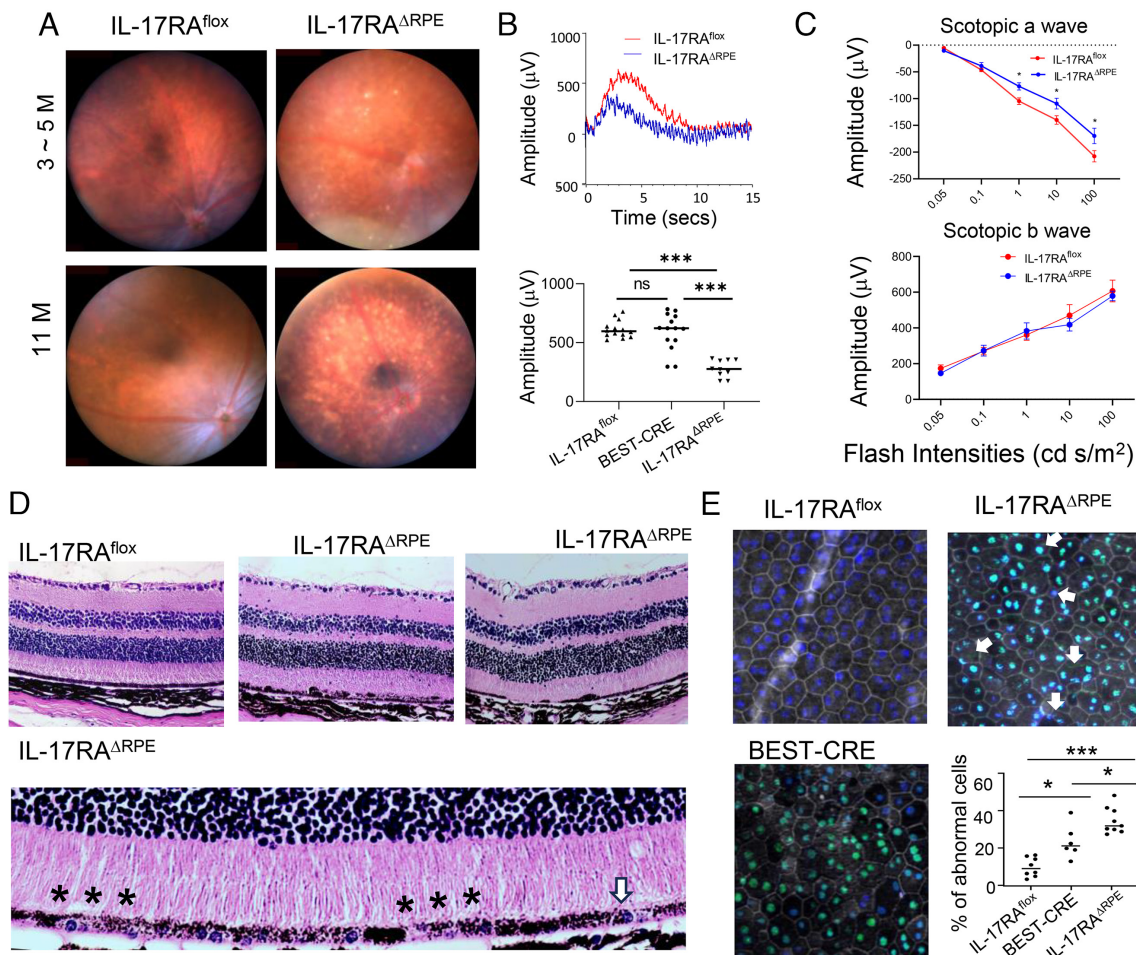


Fig. 5. Characterization of IL-17^{ΔRPE} mice. (A) Representative fundus photos were taken from IL-17RA^{flx} and IL-17RA^{ΔRPE} mice at young (3 to 6 mo) and middle ages (8 to 11 mo). (B and C) ERG c-wave and scotopic a- and b-wave measurements from mice at 8 to 10 mo of age. Data are the averages from 4 independent experiments (mean \pm SEM, N = 6 to 8) ($^*P < 0.05$ and $^{***}P < 0.001$). (D) H&E-stained paraffin sections from IL-17RA^{flx} and IL-17RA^{ΔRPE} mice at 10 to 12 mo of age, showing areas of subretinal cell infiltration, focal RPE thinning, RPE pigment loss (*), and pyknosis (arrow). (E) Immunostaining of RPE/choroid flat mount and quantitation data from IL-17RA^{flx}, IL-17RA^{ΔRPE}, and BEST-CRE mice. Green, CRE staining; gray, RPE phalloidin. Arrows indicate RPE cells with abnormal morphology.

ERG C-wave measurement, and histopathology (Fig. 5). The IL-17RA^{ΔRPE} mice are likely to be more sensitive to other insults. A main limitation of the NaIO₃ model is that it is an acute toxicity model in which all RPE cells are injured at the same time. Future studies can be performed to examine the IL-17RA^{ΔRPE} mice using chronic models, such as aging and high-fat diet (46, 47).

The current study defined a communication network involving choroidal γδ T cells, RPE, and subretinal microglia, which may provide a precisely regulated protective mechanism within the posterior eye. Choroidal γδ T cells generated IL-17, which stimulated the production of IL-6 by the RPE (Fig. 2 D and E). IL-6 activated the mTOR pathway in microglia, redirecting their energy metabolism from glucose utilization toward fatty acids oxidation (Fig. 3). Given that subretinal microglia reside in a lipid-rich microenvironment, metabolically reprogrammed microglia will overcome the immune suppressive functions of cytokines like TGF-β (48) and are primed to perform their function of clearing lipid waste products from both the RPE and photoreceptor cells (49). However, overactivation of subretinal microglia poses a threat to cone cells (50, 51). The intricate relay of the immune modulatory cytokine signals ensures finely tuned responses specifically in the vicinity of injured RPE, without causing overt toxicity. The small number of γδ T cells in the choroid minimizes the risk of excessive production of IL-17.

The effects of IL-6 on microglia include the upregulation of IL-4 receptor and potentiation of their M2a activation (Fig. 4). In the posterior eye with pathological angiogenesis, IL-4 was found to be mainly expressed by bone marrow cells that were recruited to the sites of choroidal neovascularization, and its receptor was located on Iba-1⁺ retinal microglia/macrophages (52). Therefore, activation of subretinal microglia involves interactions among several types of immune cells in a series of concerted events with tightly controlled spatial and temporal regulation. Instead of direct activation with a specific signal, the system of cytokine relay and cell–cell interaction can avoid accidental activation of myeloid cells near the retinal neurons.

In summary, results from our current study revealed a signaling cascade of choroidal γδ T cells, RPE, and subretinal microglia. The choroidal γδ T cells can sense RPE injury and produce IL-17. IL-17 in turn activates the RPE production of IL-6, which activates mTOR in subretinal microglia and ensures the proper functions of the subretinal microglia. The protective immune response confers protection on the RPE and outer retina.

Materials and Methods

Mice. Animal procedures were reviewed and approved by the Institutional Animal Care and Use Committee of the University of Oklahoma Health Sciences Center.

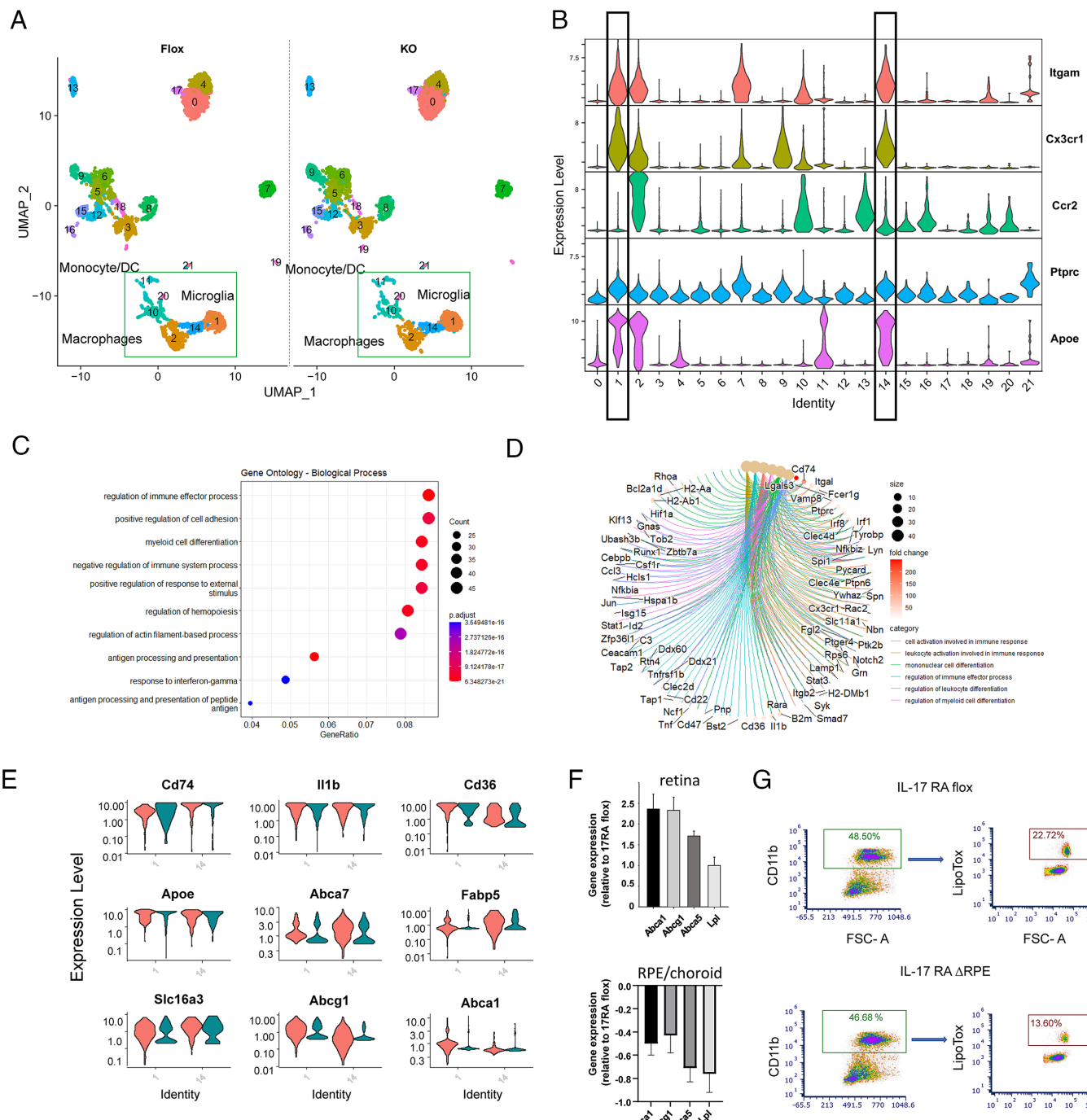


Fig. 6. Defective lipid metabolism functions of subretinal microglia in IL-17RA $^{\Delta\text{RPE}}$ mice. (A) UMAP plots of scRNA-seq data from CD45-enriched RPE/choroid preparations of IL-17RA $^{\text{flox}}$ and IL-17RA $^{\Delta\text{RPE}}$ mice. Mice were terminated at 3 d after treatment with 25 mg/kg NaO₃. (B) Violin plots showing markers of myeloid cell clusters. (C and D) Gene ontology and pathway enrichment analyses of differential gene expression between IL-17RA $^{\text{flox}}$ and IL-17RA $^{\Delta\text{RPE}}$ mice. (E) Violin plots of selected genes related to microglial lipid metabolism. (F) Real-time RT-PCR analyses of cells isolated with CD11b MACS beads. (G) Flow cytometry analyses of neutral lipid contents in CD45 $^{+}$ CD11b $^{+}$ cells from RPE/choroid preparations of IL-17RA $^{\text{flox}}$ and IL-17RA $^{\Delta\text{RPE}}$ mice.

C57BL/6J mice, IL-17RA $^{\text{flox}}$ mice (B6.Cg-IL17 $^{\text{tm}2.2\text{kO}}/\text{J}$, stock number 03100) (53), and BEST1-Cre mice (C57BL/6-Tg(BEST1-cre)1Jdun/J, stock number 017557) (54) were purchased from Jackson Laboratory (Bar Harbor, ME). All mice were fed ad libitum. Rd8 mutation in the *Crb1* gene was routinely screened (9), validated by genotyping at TransnetYX, and was not identified in these strains. All procedures were performed following the Association for Research in Vision and Ophthalmology statement for the Use of Animals in Ophthalmic and Vision Research. Mice eyes were harvested from animals killed by carbon dioxide inhalation.

Human Donor Eye Tissues. Human donor eyes with AMD or age-matched controls were obtained from Lions Gift of Sight and Minnesota Eye Bank (14). Patient

information, including age, sex, and AMD status, was described in *SI Appendix*, Table S1. All eyes were collected within 8 hours postmortem and were overnight fixed in Davidson's fixative. Antigen epitopes were retrieved by the heat-induced method in EnVision FLEX Target Retrieval Solution (Citrate buffer pH 6.1, Agilent Technologies, Inc.). Tissue autofluorescence was quenched with 0.1% Sudan Black.

Antibodies and Chemicals. Antibodies used for flow cytometry, immunostaining, and western blots were listed in *SI Appendix*, Table S2. Sodium iodate was from Sigma-Aldrich. HSC LipidTOX Red Neutral Lipid Stain dye was obtained from Invitrogen (Carlsbad, CA). Recombinant mouse IL-17 and IL-6 were from R&D Systems (Minneapolis, MN).

Flow Cytometry Analyses of Choroidal Lymphocytes. Mouse RPE/choroid/sclera tissues were collected from enucleated eyes. The anterior segment and retina were removed by microdissection. Tissues from at least 10 mouse eyes were pooled together and digested with 0.2 mg/mL collagenase D (Sigma) and dispase (StemCell) at 37 °C for 30 min. Cell clumps were removed by passing through a 40-mm cell strainer; mononuclear cells were enriched by a gradient centrifugation (9). Staining of cell surface markers and intracellular staining of IL-17A was performed as described (9), after in vitro stimulation with phorbol myristate acetate and ionomycin (Tonbo Biosciences, San Diego, CA) for 4 h. Brefeldin A was used to treat the cells in the last two hours to inhibit protein transport. Samples were analyzed on an Attune NxT flow cytometer (Thermo Fisher) (25). Compensation was performed with UltraComp eBeads (Thermo Fisher), following the manufacturer's guide. Data were processed with either FlowJo (Ashland, OR) or FCS Express (De Novo Software, Pasadena, CA).

ScRNA-seq. Single-cell suspension from collagenase D- and Dispase-digested posterior eye cups was enriched for immune cells by flow cytometry sorting of CD45⁺ viable cells at the core facility of the Oklahoma Medical Research Foundation (OMRF) (14). Barcoding, library construction, and next-generation sequencing were performed by the Genomics core of OMRF. Count matrices were generated by Cell Ranger software for 3,619 cells for IL17RA^{flx} mice and 4,092 cells for IL17RA^{ΔRPE} mice. Cells with a number of genes lower than 200, higher than 6,000, or more than 10% mitochondrial genes were excluded. Data were imported into Seurat Package and analyzed in R (14). Normalization, Clustering Uniform Approximation and Projection (UMAP) plots, and differential gene expression analyses were performed by Seurat. Candidate genes were further subjected to gene set enrichment analyses in ClusterProfiler (55) and visualized by Cnetplot function in R.

Bulk RNA Sequencing of Cultured Retinal Microglia. Retinal microglia were isolated from neonatal P3–P5 mice (25) and cultured in Dulbecco's Modified Eagle Medium (DMEM)/F12 medium supplemented with 20% fetal bovine serum (Invitrogen) and granulocyte-macrophage colony-stimulating factor (100 ng/mL) (56). Purity and cell lineage makers such as CD11b were monitored by flow cytometry (25). One week after the initial seeding, cells were lifted by gentle scraping and seeded onto 6-well culture inserts (0.4 mm pore size, Falcon) and cocultured with 10 RPE eye cups on the basal side. Recombinant mouse IL-6 (50 ng/mL) was added to the apical chamber. After 16 h, total RNA was isolated from microglial cells with Trizol Plus RNA purification kit (Thermo Fisher) and sent for next-generation sequencing by BGI Genomics (San Jose, CA). RNA-seq data were analyzed in DESeq2 (25).

Ex vivo IL-17 Stimulation of IL-6 Production. Eye cups were prepared from wild-type mice after removal of the anterior segments and retina, and were incubated in serum-free DMEM with the indicated amount of IL-17. After 16 h, the RPE/choroid tissues were harvested for RNA isolation in Trizol reagent (Invitrogen). Quantitative real-time RT-PCR was performed as described (14). To measure IL-6 secreted to the culture supernatant, RPE eye cup-conditioned medium was collected and precleared by centrifugation at 12,000 g for 5 min at 4 °C. The amount of released IL-6 was measured by ELISA (R&D Systems, Minneapolis, MN). Similar experiments were performed with primary mouse RPE cells (29) and ARPE-19 cells.

ERG. Mice were dark-adapted overnight in a temperature-controlled room and were anesthetized with ketamine/dexmedetomidine. Pupils were dilated with 0.5% tropicamide. The scotopic and photopic electrotretinograms and c-wave were

recorded with a Diagnosys Espion E2 ERG system (Diagnosys, LLC, Lowell, MA) as described previously (14).

Immunofluorescent Staining of RPE/Choroid/Sclera Flat Mounts. Enucleated mouse eyes were microdissected to remove the extraocular muscle and connective tissue, anterior segment, and the retina. Flat mount preparations were fixed in 4% paraformaldehyde and stained with anti-Cre antibody (Cell Signaling) as described (14). RPE boundaries were delineated with Alexa Fluor 647-conjugated phalloidin staining and nuclei were stained with DAPI. Images of optical sectioning were acquired from midperipheral areas on a Zeiss Axio10 microscope with Apotome and reconstructed with maximum intensity projection (14). Abnormal RPE cells were defined as 1) cells with more than two nuclei or without nucleus, 2) nuclei located on the plasma membrane, and 3) cell size more than three time larger or smaller than the average cell size in the area (30).

Seahorse Metabolic Flux Assay. Primary mouse retinal microglia were used for the metabolic assays to measure the oxygen consumption rates and extracellular acidification with glucose and palmitate-bovine serum albumin (BSA) as respiration substrates. A total of 2×10^5 cells were seeded in Seahorse 96-well microplate (Agilent, Santa Clara, CA) and treated with IL-6 or rapamycin for 16 h. MitoStress and Palmitate Oxidative Stress tests were performed following the manufacturer's guide. Normalization was performed with nuclei staining and the number of cells per well was counted by CytaCount 1 (Agilent). Data were analyzed in Wave software.

Flow Cytometry Analysis of Neutral Lipid Content in Retinal and Choroidal Immune Cells. IL17RA^{flx} and IL17RA^{ΔRPE} mice were treated with NaIO₃ at 25 mg/kg body weight by intraperitoneal injection. After 3 d, the eyes were enucleated and retina or RPE/choroidal tissues were pooled from 6 eyes. Single-cell suspension was achieved by collagenase/Dispase digestion. CD45⁺ cells were enriched with the EasySep Mouse CD45 Positive Selection Kit (Stemcell Technologies, Vancouver, BC, Canada) and further labeled with anti-CD11b antibody. Viability was measured by staining with LIVE/DEAD Fixable Near IR (780) dye (Thermo Fisher). After surface labeling, cells were fixed with 4% paraformaldehyde for 10 min, and stained with HSC LipidTOX Red neutral lipid stain at 1:1,000 dilution. Stained cells were analyzed by flow cytometry.

Statistics. Statistical analyses were performed with GraphPad Prism software. The normality of the data distribution was evaluated using the Kolmogorov-Smirnov test. Between-group differences were assessed by Student's *t* test or Mann-Whitney test, with the level of significance presented as *P* values. For multiple group comparisons, if data passed the normality test (*P* > 0.05), one-way ANOVA was used, followed by Dunnett's posttests or Sidak's Multiple comparisons test. If the data were not normally distributed, the Kruskal-Wallis test (a nonparametric alternative to ANOVA) was used, followed by Dunn's multiple comparisons tests.

Data, Materials, and Software Availability. scRNA-seq data have been deposited in GEO ([GSE244661](#)) (57).

ACKNOWLEDGMENTS. This work was supported by NIH grants R01 EY026999 (Y.C.), EY028773 (J.C.), EY034742 (J.-X.M. and J.C.), EY034510 (J.-X.M.), and EY028949 (J.-X.M.), Presbyterian Health Foundation Grants 20222421 and 20221626 (Y.C.), and BrightFocus Foundation grant M2017186 (Y.C.). We acknowledge the Vision Research Facilities (Cellular Imaging, Live Animal Imaging and Ocular Immunologic modules) supported by NIH/NEI grant P30EY027125 (PI: Callegan) and an unrestricted grant from Research to Prevent Blindness to the Dean McGee Eye Institute.

1. R. Zhou, R. R. Caspi, Ocular immune privilege. *F1000 Biol. Rep.* **2**, 3 (2010).
2. M. A. Cunningham *et al.*, Proliferative vitreoretinopathy may be a risk factor in combined macular hole/retinal detachment cases. *Retina* **33**, 579–585 (2013).
3. X. Wang *et al.*, An ocular glymphatic clearance system removes beta-amyloid from the rodent eye. *Sci. Transl. Med.* **12**, eaaw3210 (2020).
4. H. Keino, S. Horie, S. Sugita, Immune privilege and eye-derived T-regulatory cells. *J. Immunol. Res.* **2018**, 1679197 (2018).
5. D. R. Green, T. A. Ferguson, The role of Fas ligand in immune privilege. *Nat. Rev. Mol. Cell Biol.* **2**, 917–924 (2001).
6. E. G. O'Koren *et al.*, Microglial function is distinct in different anatomical locations during retinal homeostasis and degeneration. *Immunity* **50**, 723–737.e7 (2019).
7. Y. Okunuki *et al.*, Microglia inhibit photoreceptor cell death and regulate immune cell infiltration in response to retinal detachment. *Proc. Natl. Acad. Sci. U.S.A.* **115**, E6264–E6273 (2018).
8. J. B. Lin, R. S. Apte, Visualizing the heterogeneity of retinal microglia. *Immunity* **50**, 544–546 (2019).
9. Z. Zhao *et al.*, Choroidal gammadelta T cells in protection against retinal pigment epithelium and retinal injury. *FASEB J.* **31**, 4903–4916 (2017).
10. Z. Zhao *et al.*, gammadelta T cells as a major source of IL-17 production during age-dependent RPE degeneration. *Invest. Ophthalmol. Vis. Sci.* **55**, 6580–6589 (2014).
11. J. Wang, J. Iacobelli, C. Spencer, M. Saint-Geniez, Direct effect of sodium iodate on neurosensory retina. *Invest. Ophthalmol. Vis. Sci.* **55**, 1941–1953 (2014).
12. K. Mulfaul *et al.*, Toll-like receptor 2 facilitates oxidative damage-induced retinal degeneration. *Cell Rep.* **30**, 2209–2224.e5 (2020).
13. G. L. Lehmann *et al.*, Single-cell profiling reveals an endothelium-mediated immunomodulatory pathway in the eye choroid. *J. Exp. Med.* **217**, e20190730 (2020).
14. J. Cai, C. Litwin, R. Cheng, J. X. Ma, Y. Chen, DARPP32, a target of hyperactive mTORC1 in the retinal pigment epithelium. *Proc. Natl. Acad. Sci. U.S.A.* **119**, e2207489119 (2022).

15. K. J. Katschke Jr. *et al.*, Classical and alternative complement activation on photoreceptor outer segments drives monocyte-dependent retinal atrophy. *Sci. Rep.* **8**, 7348 (2018).
16. F. R. Toapanta, T. M. Ross, Complement-mediated activation of the adaptive immune responses: Role of C3d in linking the innate and adaptive immunity. *Immunol. Res.* **36**, 197–210 (2006).
17. C. Kemper *et al.*, Activation of human CD4+ cells with CD3 and CD46 induces a T-regulatory cell 1 phenotype. *Nature* **421**, 388–392 (2003).
18. V. Lyzogubov *et al.*, Complement regulatory protein CD46 protects against choroidal neovascularization in mice. *Am. J. Pathol.* **184**, 2537–2548 (2014).
19. S. L. Gaffen, Structure and signalling in the IL-17 receptor family. *Nat. Rev. Immunol.* **9**, 556–567 (2009).
20. L. Wei *et al.*, Hypomethylation of the IL17RC promoter associates with age-related macular degeneration. *Cell Rep.* **2**, 1151–1158 (2012).
21. A. Swarup *et al.*, Modulating GLUT1 expression in retinal pigment epithelium decreases glucose levels in the retina: Impact on photoreceptors and Muller glial cells. *Am. J. Physiol. Cell Physiol.* **316**, C121–C133 (2019).
22. Y. Ke, G. Jiang, D. Sun, H. J. Kaplan, H. Shao, Retinal Astrocytes respond to IL-17 differently than Retinal Pigment Epithelial cells. *J. Leukocyte Biol.* **86**, 1377–1384 (2009).
23. D. Y. Chong *et al.*, Interleukin-6 as a photoreceptor neuroprotectant in an experimental model of retinal detachment. *Invest. Ophthalmol. Visual Sci.* **49**, 3193–3200 (2008).
24. S. Droho, C. M. Cuda, H. Perlman, J. A. Levine, Macrophage-derived interleukin-6 is necessary and sufficient for choroidal angiogenesis. *Sci. Rep.* **11**, 18084 (2021).
25. D. R. Morris *et al.*, Exosomal MiRNA transfer between retinal microglia and RPE. *Int. J. Mol. Sci.* **21**, 3541 (2020).
26. I. S. Junttila, Tuning the cytokine responses: An update on interleukin (IL)-4 and IL-13 receptor complexes. *Front. Immunol.* **9**, 888 (2018).
27. R. Hurdayal, F. Brombacher, Interleukin-4 receptor alpha: From innate to adaptive immunity in murine models of cutaneous leishmaniasis. *Front. Immunol.* **8**, 1354 (2017).
28. M. Z. Zhang *et al.*, IL-4/IL-13-mediated polarization of renal macrophages/dendritic cells to an M2a phenotype is essential for recovery from acute kidney injury. *Kidney Intern.* **91**, 375–386 (2017).
29. Y. M. Go *et al.*, mTOR-initiated metabolic switch and degeneration in the retinal pigment epithelium. *FASEB J.* **34**, 12502–12520 (2020), 10.1096/fj.202000612R.
30. D. Ortonan *et al.*, Single-cell-resolution map of human retinal pigment epithelium helps discover subpopulations with differential disease sensitivity. *Proc. Natl. Acad. Sci. U.S.A.* **119**, e2117553119 (2022).
31. S. M. Majka *et al.*, Analysis and isolation of adipocytes by flow cytometry. *Methods Enzymol.* **537**, 281–296 (2014).
32. J. C. Ribot, N. Lopes, B. Silva-Santos, gammadelta T cells in tissue physiology and surveillance. *Nat. Rev. Immunol.* **21**, 221–232 (2021).
33. R. L. O'Brien, W. K. Born, Dermal gammadelta T cells—What have we learned? *Cell Immunol.* **296**, 62–69 (2015).
34. A. S. Ismail *et al.*, Gammadelta intraepithelial lymphocytes are essential mediators of host-microbial homeostasis at the intestinal mucosal surface. *Proc. Natl. Acad. Sci. U.S.A.* **108**, 8743–8748 (2011).
35. M. Ribeiro *et al.*, Meningeal gammadelta T cell-derived IL-17 controls synaptic plasticity and short-term memory. *Sci. Immunol.* **4**, eaay5199 (2019).
36. K. Alves de Lima *et al.*, Meningeal gammadelta T cells regulate anxiety-like behavior via IL-17a signaling in neurons. *Nat. Immunol.* **21**, 1421–1429 (2020).
37. D. Liang *et al.*, CD73 expressed on gammadelta T Cells shapes their regulatory effect in experimental autoimmune uveitis. *PLoS One* **11**, e0150078 (2016).
38. H. Nian *et al.*, Activated gammadelta T cells promote the activation ofuveitogenic T cells and exacerbate EAU development. *Invest. Ophthalmol. Visual Sci.* **52**, 5920–5927 (2011).
39. S. R. Planck, X. N. Huang, J. E. Robertson, J. T. Rosenbaum, Retinal pigment epithelial cells produce interleukin-1 beta and granulocyte-macrophage colony-stimulating factor in response to interleukin-1 alpha. *Curr. Eye Res.* **12**, 205–212 (1993).
40. K. Spekker-Bosker, C. M. Ufermann, M. Oldenburg, W. Daubener, S. K. Eller, Interplay between IDO1 and iNOS in human retinal pigment epithelial cells. *Med. Microbiol. Immunol.* **208**, 811–824 (2019).
41. S. Kadow *et al.*, Aryl hydrocarbon receptor is critical for homeostasis of invariant gammadelta T cells in the murine epidermis. *J. Immunol.* **187**, 3104–3110 (2011).
42. B. Martin, K. Hirota, D. J. Cua, B. Stockinger, M. Veldhoen, Interleukin-17-producing gammadelta T cells selectively expand in response to pathogen products and environmental signals. *Immunity* **31**, 321–330 (2009).
43. K. L. Chu, N. V. Batista, M. Girard, T. H. Watts, Monocyte-derived cells in tissue-resident memory T cell formation. *J. Immunol.* **204**, 477–485 (2020).
44. A. Ogawa, A. Andoh, Y. Araki, T. Bamba, Y. Fujiyama, Neutralization of interleukin-17 aggravates dextran sulfate sodium-induced colitis in mice. *Clin. Immunol.* **110**, 55–62 (2004).
45. J. Wang *et al.*, Rapid onset of inflammatory bowel disease after receiving secukinumab infusion. *ACG Case Rep. J.* **5**, e56 (2018).
46. J. K. Sterling *et al.*, Inflammatory adipose activates a nutritional immunity pathway leading to retinal dysfunction. *Cell Rep.* **39**, 110942 (2022).
47. C. B. Toomey, U. Kelly, D. R. Saban, C. Bowes Rickman, Regulation of age-related macular degeneration-like pathology by complement factor H. *Proc. Natl. Acad. Sci. U.S.A.* **112**, E3040–E3049 (2015).
48. T. Zoller *et al.*, Silencing of TGFbeta signalling in microglia results in impaired homeostasis. *Nat. Commun.* **9**, 4011 (2018).
49. B. A. Loving, K. D. Bruce, Lipid and lipoprotein metabolism in microglia. *Front. Physiol.* **11**, 393 (2020).
50. S. K. Wang, Y. Xue, C. L. Cepko, Microglia modulation by TGF-beta1 protects cones in mouse models of retinal degeneration. *J. Clin. Invest.* **130**, 4360–4369 (2020).
51. J. Di Pierdomenico, D. Garcia-Ayuso, M. Agudo-Barriuso, M. Vidal-Sanz, M. P. Villegas-Perez, Role of microglial cells in photoreceptor degeneration. *Neural. Regen. Res.* **14**, 1186–1190 (2019).
52. T. Baba *et al.*, Role of IL-4 in bone marrow driven dysregulated angiogenesis and age-related macular degeneration. *eLife* **9**, e54257 (2020).
53. P. Kumar *et al.*, Intestinal interleukin-17 receptor signaling mediates reciprocal control of the gut microbiota and autoimmune inflammation. *Immunity* **44**, 659–671 (2016).
54. J. Iacovelli *et al.*, Generation of Cre transgenic mice with postnatal RPE-specific ocular expression. *Invest. Ophthalmol. Visual Sci.* **52**, 1378–1383 (2011).
55. T. Wu *et al.*, clusterProfiler 4.0: A universal enrichment tool for interpreting omics data. *Innovation (Camb)* **2**, 100141 (2021).
56. H. O Dikmen *et al.*, GM-CSF induces noninflammatory proliferation of microglia and disturbs electrical neuronal network rhythms in situ. *J. Neuroinflammation* **17**, 235 (2020).
57. J. Cai *et al.*, Interleukin-17-mediated protective cytokine signaling against degeneration of the retinal pigment epithelium. NCBI Gene Expression Omnibus. <https://www.ncbi.nlm.nih.gov/geo/query/acc.cgi?acc=GSE244661>. Deposited 4 October 2023.